Oil Shale, 2010, Vol. 27, No. 2, pp. 147–163
doi: 10.3176/oil.2010.2.05
ISSN 0208-189X

NUMERICAL SIMULATION OF UPRISING TURBULENT FLOW BY 2D RANS FOR FLUIDIZED-BED CONDITIONS

I. KRUPENSKI[(a)], A. KARTUSHINSKY[(b)*], A. SIIRDE[(a)], Ü. RUDI[(b)]

[(a)] Tallinn University of Technology
Faculty of Mechanical Egineering, Departament of Thermal Engineering
Kopli 116, 11712 Tallinn, Estonia

[(b)] Tallinn University of Technology
Faculty of Science, Laboratory of Multiphase Media Physics
Akadeemia tee 21E, 12618 Tallinn, Estonia

2D RANS (Reynolds Average Navier Stokes) equations are used for numerical modeling of uprising particulate (gas-solid particle) turbulent flow in conditions of fluidized beds. The two-fluid model approach was used in giving numerical simulations. The flow domain is a round pipe with diameter of 1 m and height of 6 m (a real industrial object). The flow of mean velocity 4 m/s carries solid particles (material density 2000 kg/m^3; sizes of 0.3, 1 and 1.5 mm) with mass flow ratio 10 kg/kg.

The mathematical model pertains to gravitational and viscous drag forces, Magnus and Saffman lift forces, effects of inter-particle collisions as well as particle interaction with the wall, effect of turbulence modulation (turbulence enhancement) at particles' presence. The fluidized-bed conditions consider that flow conditions were set for high-temperature flow, density of the carrier fluid 0.329 kg/m^3, and kinematic viscosity $1.55 \cdot 10^{-4}$ m^2/s.

The results are presented in the form of distribution of axial and radial velocity components of gaseous and solid phases, particle mass concentration and kinetic turbulent energy along the flow height at the flow exit (highest downstream position) and in the middle cross-section (intermediate position) in order to observe development of particulate flow.

As shown by the results, the 2D RANS model qualitatively and quantitatively describes the real-time distribution of flow in a real flow domain, i.e. the model covers reasonable physical phenomena occurring in fluidized-bed conditions.

* Corresponding author: e-mail *aleksander.kartusinski@ttu.ee*

Introduction

In accordance with a widespread introduction of CFB (circulating fluidized bed) furnaces in power plants, the concentration of solid ash particles in furnace gases substantially increases. The ash particles of the pulverized-firing boilers can be observed in the furnace gases as an inconvenient admixture. These particles pose specific problems such as the behaviour of inorganic matter in combustion process, fouling, high temperature corrosion and wear of the steam boiler heating surfaces. In the CFB furnaces solid ash particles are used mainly as the solid heat carrier – separated in hot cyclone and cooled in heat exchanger ash particles return to the furnace. The circulating ash mass holds the temperature level in furnace in the given range. As heat capacity of ash is quite low, the mass of circulating ash must be high. High ash concentration in furnace gases is attained a) by high velocity of gas in the bed and by the fact that most of fuel particles carried out of the bed are burned and their ash fills the whole volume of the furnace and b) by ash circulation. The CFB combustion technology enables to bind sulphur components with carbonate components added to the fuel or existing within its mineral part [1].

This article is a sequel to the previous reference: “Numerical simulation of uprising gas-solid particle flow in circulating fluidized bed” [2]. In that work the flow of gas-solid particles in conditions of CFB was studied, taking into account the amount of heat that must be separated from the combustor by the sensible heat of solid ash particles. The approach enabled to optimize mass concentration of solid ash particles in fire gases. For the numerical simulation of the uprising gas-solid particle flow occurring in the vertical riser, the CFB conditions, namely temperature, gas velocity and particles concentration, were followed, and the particles of the Estonian oil shale ash (particle size, density) were chosen.

The next simplifications were applied for numerical simulations of the uprising gas-solid particle flow: 1) the calculations concern the upper part of the furnace before the exit region, 2) the cross-section of the furnace is circular, 3) furnace gases contain only the ash solid particles taken part in the circulation process, 4) the actual gas velocity chosen equaled up to 5.5 m/s, and 5) for calculations the small-size and coarse ash particles within three different medium size intervals were chosen.

The previous numerical simulations were performed using the two-phase turbulent boundary layer (TBL) approach [2]. This implies that the diffusive source terms were retained only in one direction, namely in the transverse one, and the magnitude of the average transverse velocity components of the gas- and dispersed phases was much less than that of the longitudinal components of the corresponding velocities of gaseous and dispersed phases. Such approach is thoroughly valid and used in the case of pipe channel flows as well as in the turbulent round jets [3–5].

The present work is the first implementation of the numerical 2D RANS approach (Reynolds Average Navier-Stokes equations) for running the turbulent particulate flow in conditions of a real CFB furnace with the initial data obtained at combusting Estonian oil shale. By the given mathematical prediction (2D RANS approach) we replaced the former TBL approach in order to rigorously describe the complicated physical thermodynamic process in a real-size CFB unit. In the case of the Eulerian approach, the original collision model was used for the closure of transport equations by accounting the inter-particle collision effect occurring in CFB due to high mass loading [6]. The numerical parametric study deals with the influence of parameters of various riser exits on the hydrodynamics of the gas-solid two-phase flow taking place in the riser of CFB [7, 8]. The problems of two-phase flows in the CFB risers are analyzed in publications, but these studies do not consider the dependence of the amount of the sensible heat carried by solid ash particles on their concentration in gases.

Unlike our previous article, the following practical initial data were used in calculations:

Table 1. **The initial data for calculations**

Parameters		Dimension	Minimal	Average	Maximal
Pipe data	Diameter	m	1	1	1
	Height	m	6	6	6
Ash concentration		kg/nm^3	10	15	20
Ash density		kg/m^3	2000	2000	2000
Particle size		m	0.0003	0.001	0.0015
Temperature		°C	750		850
Gas data	Additives	CO_2, H_2O, N_2	–	–	–
	Speed	m/s	4	4	4
	Density	kg/m^3	0.329	0.329	0.329
Viscosity		mm^2/s	0.000155	0.000155	0.000155

The differences from our previous work are substantial in respect of the use of mathematical modeling and in respect of selection of the flow domain which is close to reality. Besides, particles are coarser, ash is heavier and flue gas velocity is slightly slower. We chose initial data of two-phase medium which are very close to a CFB furnace burning Estonian oil shale.

The present research is a continuation of our previous numerical study of processes occurring in CFB using the two-fluid (Euler-Euler) approach to describe the behavior of solid particles as a continuous co-existing solid phase. To evaluate the input of real effects taking place in dispersed phase in CFB, an industrial CFB unit is used here as the two-phase flow domain occupied by the mixture of gas and particles. The domain is considered to be a cylindrically symmetric pipe section. Along with this the 2D RANS modeling together with the use of finite (control) volume method [9, 10] is currently applied to avoid common assumptions of turbulent boundary layer

"TBL" approximation. We extended RANS modeling originally performed for 2D single-phase turbulent pipe flow, covering now the two-phase flow with an incorporated solid particle phase. The other popular approach in use now for modeling the dispersed phase is the Lagrange particle tracking method. When using the Lagrange method one must handle a huge number of tracking particles (up to several millions of particles depending on mass flow loading) to obtain solution convergence, and for taking into account particles feedback into the primary (gas-phase) fluid, average velocities and turbulence one can use the particle-cell source method [11], unlike the Euler approach it enables to consider the direct impact of particles on fluid turbulent structure. The two-dimensional flow of gas-solid particles taking place in the CFB riser (total volume concentration of solids 3%) was studied by the Lagrangian approach using the particles tracking method [12]. The Lagrangian approach of particle collisions was used also in [13] where a stochastic inter-particle model was introduced to describe collision of fictitious particles and trace particles.

Theoretical terms of model

In the field of non-isothermal multiphase flows there were developed a lot of models for particulate flows [14, 15]. The "Two-fluid model" is being used in modeling of dispersed two-phase systems, where gas and particles are considered to be two coexisting phases that reach the entire flow domain. To describe the flow of the particulate phase, one of the possibilities is using the Reynolds-Averaged Navier-Stokes (RANS) method. The general equations of this method were examined by plenty of experiments, which showed that using this method it is possible to discover, for example, boundary conditions, and it is quite easy to implement it numerically. In this work we use the RANS method with its closure equations to find data needed for the output: axial and radial velocities, turbulent energy, mass concentration. The information on these parameters will surely be useful for predicting particulate flow.

In order to take into account collision of particles in highly loaded CFB domain, the dispersed phase is presented as a polydispersed phase where collisions between the particles occur due to variation in particles size and their turbulent fluctuation motion [6]. To simplify collision of particles there are introduced three particle fractions with different particle sizes and mass fractions: $\delta_1 < \delta_2 < \delta_3$, $\beta = \beta_1 + \beta_2 + \beta_3 = 1$, where indices 1, 2, 3 are related to the first, second (main by mass loading) and third particle fractions with respect to their corresponding mass loading, β.

Governing equations and boundary conditions for the two-dimensional RANS model:

This model is based on the complete averaged Navier-Stokes equations, without any simplifications, such as "boundary layer" simplifications.

A short presentation of the governing equations for the axisymmetric pipe case is as follows:

1. Continuity for the gaseous phase:

$$\frac{\partial u}{\partial x}+\frac{\partial (rv)}{r\partial r}=0$$

2. Linear momentum equation in the axial direction for the gaseous phase:

$$\frac{\partial}{\partial x}\left(u^2-\nu_t\frac{\partial u}{\partial x}\right)+\frac{\partial}{r\partial r}r\left(uv-\nu_t\frac{\partial u}{\partial r}\right)$$
$$=-\frac{\partial p}{\rho\partial x}+\frac{\partial}{\partial x}\nu_t\frac{\partial u}{\partial x}+\frac{\partial}{r\partial r}r\nu_t\frac{\partial v}{\partial x}-\sum_{i=1,3}\alpha_i\left(\frac{u_{ri}}{\tau_i'}+C_{Mi}\Omega_i v_{ri}\right)$$

3. Linear momentum equation in the radial direction for the gaseous phase:

$$\frac{\partial}{\partial x}\left(uv-\nu_t\frac{\partial v}{\partial x}\right)+\frac{\partial}{r\partial r}r\left(v^2-\nu_t\frac{\partial v}{\partial r}\right)$$
$$=-\frac{\partial p}{\rho\partial r}+\frac{\partial}{\partial x}\nu_t\frac{\partial u}{\partial r}+\frac{\partial}{r\partial r}r\nu_t\frac{\partial v}{\partial r}-\frac{2\nu_t v}{r^2}-\sum_{i=1,3}\alpha_i\left(\frac{v_{ri}}{\tau_i'}-(C_{Mi}\Omega_i+F_{si})u_{ri}\right)$$

4. Turbulence kinetic energy equation for the gaseous phase:

$$\frac{\partial}{\partial x}\left(uk-\nu_t\frac{\partial k}{\partial x}\right)+\frac{\partial}{r\partial r}\left(vk-\nu_t\frac{\partial k}{\partial r}\right)$$
$$=\nu_t\left\{2\left[\left(\frac{\partial u}{\partial x}\right)^2+\left(\frac{\partial v}{\partial r}\right)^2+\left(\frac{v}{r}\right)^2\right]+\left(\frac{\partial u}{\partial r}+\frac{\partial v}{\partial x}\right)^2\right\}-\varepsilon_h$$
$$+\sum_{i=1,3}\frac{\alpha_i}{\tau_i}\left(u_{ri}^2+v_{ri}^2+0.5(\overline{u_{si}'^2}+\overline{v_{si}'^2})_c-\frac{k}{\left(1+\frac{\tau_i}{\mathrm{T}_0}\right)}\right)$$

5. Momentum equation in the axial direction for the solid phase:

$$\frac{\partial}{\partial x}(\alpha_i u_{si}u_{si})+\frac{\partial}{r\partial r}(r\alpha_i u_{si}v_{si})$$
$$=-\frac{\partial}{\partial x}\left(\alpha_i\overline{u_{si}'^2}\right)-\frac{\partial}{r\partial r}\left(r\alpha_i\overline{u_{si}'v_{si}'}\right)+\alpha_i\left[\frac{u_{ri}}{\tau_i'}+C_{Mi}\Omega_i v_{ri}-g\left(1-\frac{\rho}{2\rho_p}\right)\right]$$

6. Momentum equation in the radial/transverse direction for the solid phases:

$$\frac{\partial}{\partial x}\left(\alpha_i v_{si} u_{si}\right)+\frac{\partial}{r\partial r}\left(r\alpha_i v^2{}_{si}\right)$$
$$=-\frac{\partial}{\partial x}\left(\alpha_i \overline{u'_{si}v'_{si}}\right)-\frac{\partial}{r\partial r}\left(r\alpha_i \overline{v'^2_{si}}\right)+\alpha_i\left[\frac{v_{ri}}{\tau'_i}-\left(C_{Mi}\Omega_i+F_{si}\right)u_{ri}\right]$$

7. Linear momentum equation in the axial direction for the solid phases:

$$\frac{\partial}{\partial x}\left(\alpha_i \omega_{si} u_{si}\right)+\frac{\partial}{r\partial r}\left(r\alpha_i \omega_{si} v_{si}\right)$$
$$=-\frac{\partial}{\partial x}\left(\alpha_{si}\overline{u'_{si}\omega'_{si}}\right)-\frac{\partial}{r\partial r}\left(r\alpha_{si}\overline{v'_{si}\omega'_{si}}\right)-\alpha_i C_{\omega i}\frac{\Omega_i}{\tau_i}$$

The main force factors included in numerical simulation of the considered process in CFB are viscous drag force expressed *via* particles' response time, $\tau'_i=\tau_i/C'_{Di}$, two lift forces Saffman *via* coefficient, F_{si} and Magnus, through coefficient, C_{Mi}, gravitational force determined by grafitational acceleration, *g*. In addition there are inter-particle collision expressed via collisional stresses (velocity correlations, $\overline{u'^2_{si}}$, $\overline{v'^2_{si}}$, $\overline{u'_{si}v'_{si}}$ $\overline{u'_{si}\omega'_{si}}$, $\overline{v'_{si}\omega'_{si}}$) and turbulence modulation described by four-way coupling [16] model (k-eq. 4). One of the main characteristics (shape factor, etc) of solid particles, observed in a CFB furnace, is investigated and presented in [17].

The boundary conditions are as follows.

Inlet boundary (x = 0):

It is assumed that the particles enter into previously computed, single-phase velocity field with an initial velocity lag determined by coefficient k_{lag}:

$$u_{si}=k_{lag}u,\quad v_{si}=k_{lag}v,\quad \omega_{si}=k_{lag}\left(0.5rot\vec{v}\right).$$

Wall and centerline conditions:

The wall-function procedure is applied at the wall for axial velocity, turbulent energy and its rate of dissipation, while at the center the axisymmetric conditions are applied:

$$r=0:\ \frac{\partial u}{\partial r}=\frac{\partial k}{\partial r}=\frac{\partial u_{si}}{\partial r}=\frac{\partial \alpha_i}{\partial r}=v=v_{si}=\omega_{si}=0,$$

$$r=R:\ u=u_\tau\left(\frac{1}{\kappa}\ln y^+ +5.2\right),\ v=0,$$

$P = \tau_w \dfrac{\partial u}{\partial y} = \dfrac{2\tau_w^2}{\kappa c_\mu^{0.25} \sqrt{k\left(x, R - \dfrac{\Delta}{2}\right)}\Delta}$ is production of the turbulent energy that determines turbulent energy at the wall;

$$\varepsilon = c_\mu^{0.75} \frac{2k^{1.5}\left(x, R - \dfrac{\Delta}{2}\right)}{\kappa\Delta},$$

where

$$u_\tau = c_\mu^{0.25}\sqrt{k}\,, \quad y^+ = \frac{u_\tau y}{\nu} = \frac{c_\mu^{0.25}\sqrt{k\left(x, R - \dfrac{\Delta}{2}\right)}\Delta}{2\nu}\,, \quad \tau_w = \frac{\kappa c_\mu^{0.4}\sqrt{k}}{\ln(Ey^+)} u\left(x, R - \frac{\Delta}{2}\right),$$

Δ is the numerical step grid.

The slip boundary condition for the dispersed phase is prescribed according to the model in [18] as the first step in the computations. Subsequently, we followed the procedure given in [19] to determine the particle-wall interactions occurring before and after the particle collisions with the walls. Accordingly, we have two cases of particle-wall interactions a) sliding collisions, and b) non-sliding collisions. These two cases are characterized by the coefficients of restitution, k_n, and friction, *f*.

For *sliding collisions* we have the wall boundary condition:

$$r = R:\; u_{si} = -\lambda_i \frac{\partial u_{si}}{\partial r}\,,\; v_{si} = -\lambda_i \frac{\partial v_{si}}{\partial r}\,,\; \omega_{si} = \lambda_i \frac{\partial \omega_{si}}{\partial r}\,,$$

where the inter-particle spacing is given by the closure equation:

$$\lambda_i = d_i \left\{ \left[\frac{\pi}{6}\left(\frac{\rho_p}{\rho\alpha_i} + 1 \right) \right]^{1/3} - 1 \right\}.$$

If the transverse particle velocity is positive ($v_{si} > 0$), the correction suggested by [20] is used. Therefore, if $\left|u_{si} - 0.5 d_i \omega_{si}\right| > 3.5\mu_0 \left(1 + k_n\right) v_{si}$, the boundary conditions for sliding collisions are as follows:

a) $u'_{si} = u_{si} + \mu_d \operatorname{sign}\left(u_{si} - 0.5 d_i \omega_i\right) v_{si}\,,$

$\omega'_{si} = \omega_{si} + \left(5\mu_d \operatorname{sign}\left(u_{si} - 0.5 d_i \omega_i\right) \dfrac{v_{si}}{d_i} \right),$

$v''_{si} = k_n v_{si}$

For *non-sliding collisions* the condition $\left|u_{si} - 0.5 d_i \omega_{si}\right| \le 3.5\mu_0 \left(1 + k_n\right) v_{si}$ is satisfied, and the boundary conditions of the dispersed phases at the wall may be written as:

b) $u'_{si} = u_{si} - \frac{2}{7}(u_{si} - 0.5 d_i \omega_i)$, $\omega''_{si} = \omega_{si} - \frac{10(u_{si} - 0.5 d_i \omega_i)}{7 d_i}$, $v''_{si} = k_n v_{si}$,

where the primes denote that the corresponding variables are to be calculated after collision.

In the axial direction at the flow exit:

$$\frac{\partial u}{\partial x} = \frac{\partial v}{\partial x} = \frac{\partial u_{si}}{\partial x} = \frac{\partial v_{si}}{\partial x} = \frac{\partial \omega_{si}}{\partial x} = \frac{\partial \alpha_i}{\partial x} = \frac{\partial k}{\partial x} = 0 .$$

Results and discussions

Numerical method: In the RANS computations the *control volume* method was used. The governing equations (1–8) were solved by using the ILU method, which incorporates a strong implicit procedure with lower and upper matrix decomposition and with an up-wind scheme. As for ILU method, the *L* and *U* matrices have non-zero elements only on diagonals on which matrix A has no-z*ero elements, M = LU = A + N* [7, 8]. The elements of the matrices *L* and *U* need to be calculated only once prior to the first iteration. On subsequent iterations one calculates only residual matrix solving the two tridiagonal systems. The rate of convergence 10^{-3} and the number of steps for total convergence mainly depend on flow domain size and in the considered case it was up to 15,000 steps. For the computations presented in this paper, 600,000 uniformly sized volumes were used. The wall functions, obtained from [7] were incorporated at a dimensionless distance *y+* = 11 from the wall. All computations were extended from the pipe entrance to a distance *x/D* = 30. For the particulate phases, where the size of particles is often larger than the size of the viscous boundary sublayer we employed the numerical method developed by Hussainov et al. [4] and used wall functions to set gas-phase axial velocity and turbulent energy required for 2D RANS approach. All results are presented in dimensionless way: the velocities of both phases are related to gas-phase velocity at the center of flow (*r* = 0), turbulent energy – to square of gas-phase velocity at flow center, particle mass concentration – to its value at flow domain center (*r* = 0).

Numerical results. It is known that the increase in the particle mass concentration as well as the decrease in the particle size result in the decrease in the velocity slip between average velocities of gas and dispersed phases [4]. The effect of the interparticle collisions is very important for the particulate flows of the mass ratio larger than 1 kg dust/kg air, $\tau_c / \tau_p < 1$, in which case the time of interparticle collision τ_c is less than the particle response time τ_p. We performed calculations taking into account the interparticle collisions with introduction of Reynolds stresses of the dispersed phase. These stresses are not empirical or semi-empirical constants (Eq. (6)), they are obtained by

analytical solution of an original model of closure which is based on the particle collisions [6].

The results of the simulation are shown in figures. In Fig. 1 there are axial velocities of carrier fluid (gas-phase) and dispersed phase in case diameter of solid particles is 0.3 mm, calculated for different flow conditions – with and w/o particle collisions. As one can notice, the results of particle collision align with velocity profiles of the dispersed phase. In the poly-dispersion case there is observed a smaller velocity slip between gas-phase and average velocity of the dispersed phase over three particle fractions. This is due to the presence of smaller particle fraction among other "mean" and "large" particle fractions in the composition of the polydispersed phase which differs from the case of monofraction particle fractions' composition of the same particle sizes. Eventually it produces a larger drag than polydispersed solid phase motion.

Figure 2 shows that radial velocity of both phases increases off the axis, and the magnitude is highest somewhere in the middle of the flow cross-section. This radial velocity of the dispersed phase results in redistribution of particle mass concentration in cross-sections of the flow. In both cases of the motion of monodispersed and polydispersed particles (collision motion) the important role of radial velocity of the dispersed phase should be taken into account. The effect of particle collisions levels the radial velocity of dispersed phases.

Figure 3 shows the distribution of turbulence at motion of relatively small solid particles of 0.3 mm for two regimes – with and without particle collisions. One can indicate that the presence of particles leads to turbulence enhancement in the turbulent core and in the wall vicinity in comparison with the case of the single-phase flow. It follows from the four-way coupling

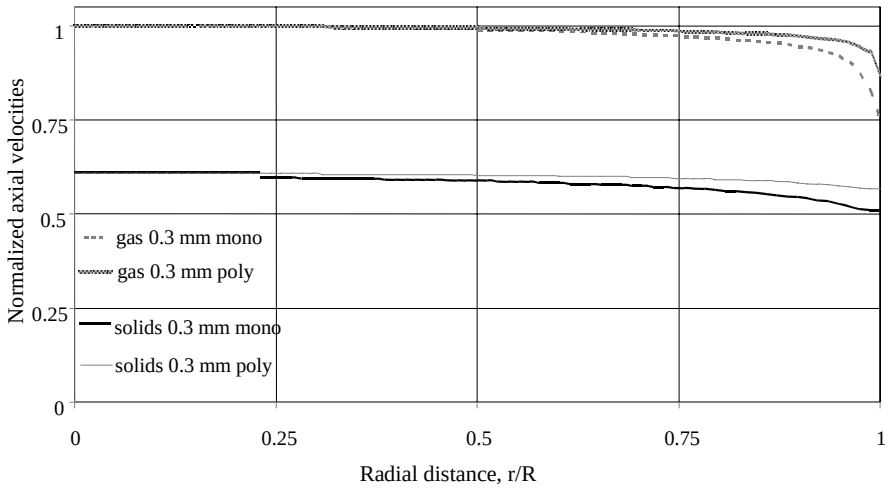

Fig. 1. Axial velocity distribution of gas- and dispersed phases for particles (0.3 mm) with and without collision effect.

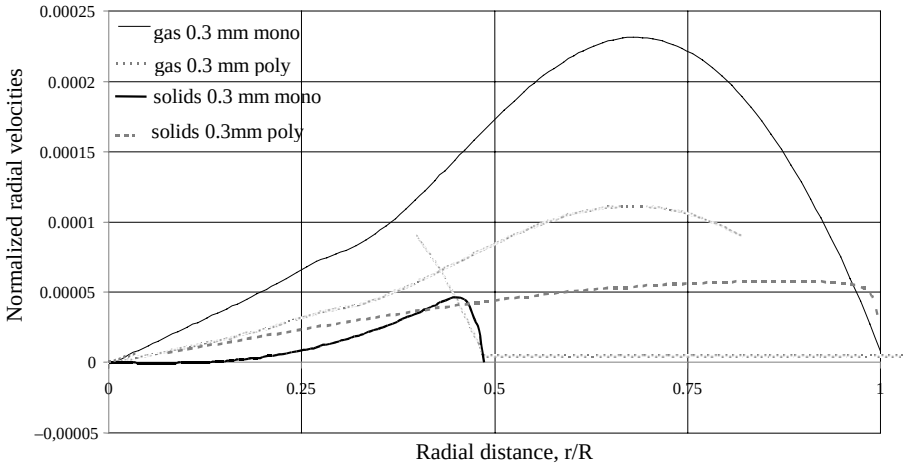

Fig. 2. Radial velocity profiles of gas- and dispersed phases for particles (0.3 mm) with and without collision effect.

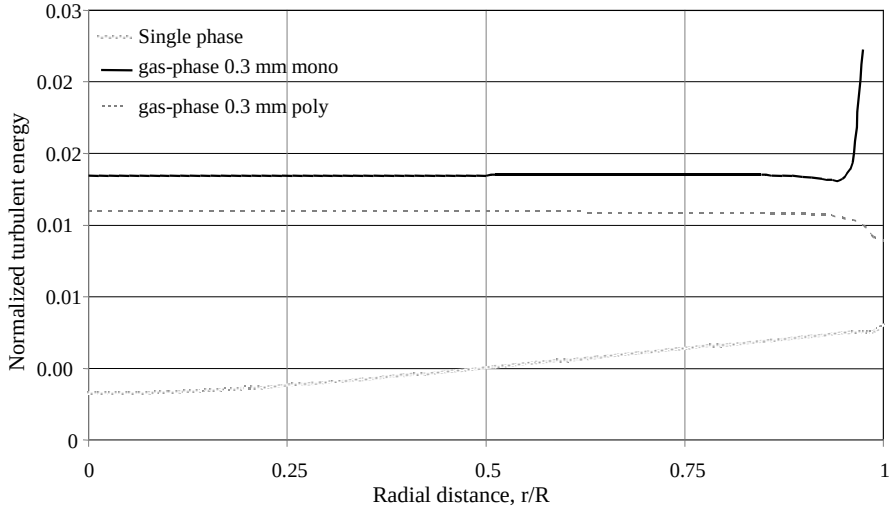

Fig. 3. Turbulent energy profiles of single and gas phases for particles (0.3 mm) with and without collision effect.

model [16] where along with average velocity slip due to gravitation force there occurs interparticle collision by which the particles decelerate downward uprising flow. The physics behind this is the formation of vortex shedding which generates additional turbulent energy due to the particles' presence. This process is less pronounced in the case of the polydispersed phase with lower level of additional turbulence generation than in the case of the monodispersed phase because of smaller velocity slip occurring at the motion of the polydispersed phase (Fig. 1).

Figure 4 shows the distribution of the mass concentration for small particles (0.3 mm) with and without particle collisions. The profiles of particle mass concentration are almost flat with slightly decreases in distribution of mass concentration towards the wall in the case of the polydispersed phase. In this case the coefficient of turbulent diffusion of particles is sufficiently large to unify the particles' mass distribution across the flow.

The following case with larger particles of 1 and 1.5 mm shows an increase in velocity slip between phases in comparison with the previous case with smaller sizes of particles, and it is observed in both axial radial directions (Figs. 5 and 6). So, the mathematical model gives reasonable results of profiles of flow parameters (averaged velocities of gaseous and dispersed phases, turbulent energy).

Figure 7 shows two *k*-profiles (turbulent energy) at motion of relatively large particles of 1 and 1.5 mm. The presence of large particles may cause a noticeable effect on turbulence redistribution generating the turbulence growth for motion of larger particles of 1.5 mm in comparison with relatively smaller particles 1 mm (Fig. 7). It results from the velocity lag which is larger for 1.5 mm particles than for 1 mm particles.

In the case of larger particles of 1.5 mm one can see the jump in distributions of axial (Fig. 5) and radial velocity of solids (Fig. 6) together with particle mass concentration (Fig. 8). To describe the motion of coarse particles in the wall vicinity with zero velocity of carrier fluid approaching to the wall it should be noted that such coarse particles are in the area close to the wall where gas velocity differs from zero to hold the motion of coarse

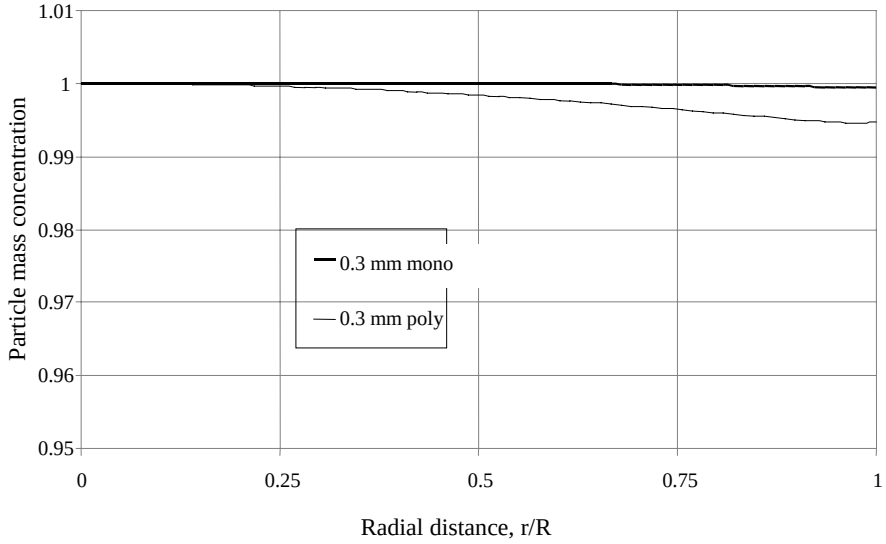

Fig. 4. Mass concentration distribution for particles (0.3 mm) with and without collision effect.

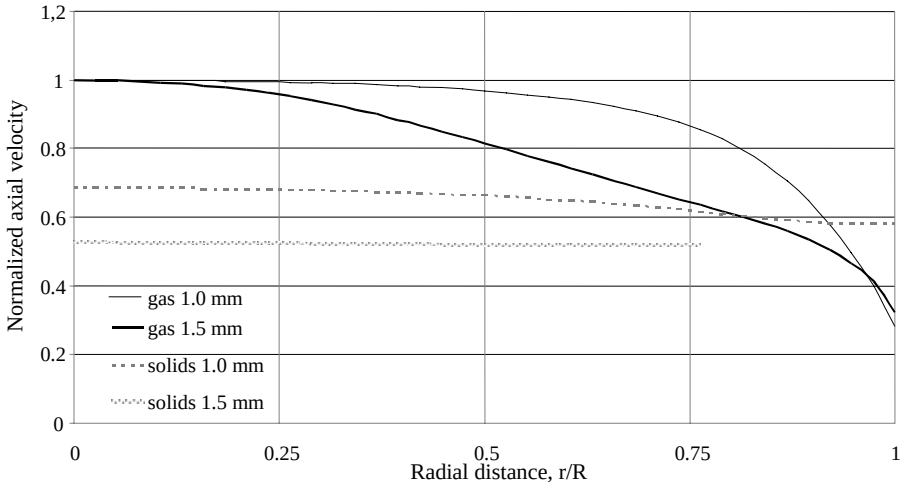

Fig. 5. Axial velocity profiles of gas- and dispersed phases for different particle sizes (1.0 and 1.5 mm).

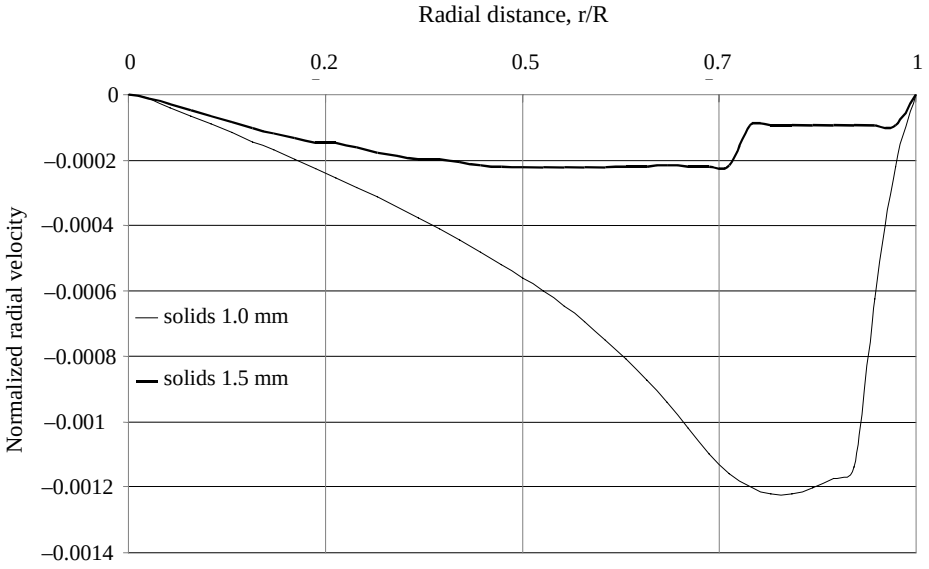

Fig. 6. Radial velocity profiles for different particle sizes (1.0 and 1.5 mm).

particles upward with gas velocity exceeding “gravitational” velocity of particles (particles velocity due to their gravitation). For this case the model given in [4] is employed.

The high level of additional production of turbulent energy by rough particles is the result of high velocity slip in a turbulent core of the flow as

well as a substantial velocity slip in the wall region. In both given cases of 1 and 1.5 mm, the presence of such rough solid particles results in turbulence enhancement in comparison with the single-phase flow.

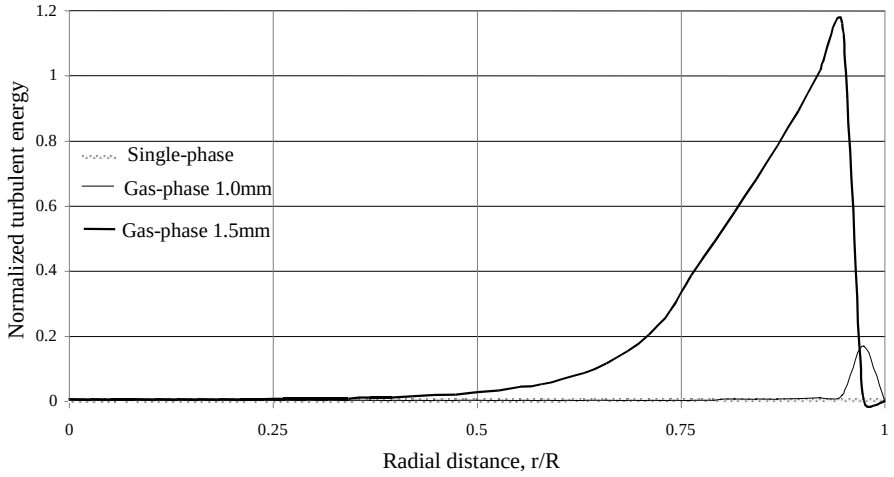

Fig. 7. Turbulent energy profiles of single and gas phases for different particle sizes (1.0 and 1.5 mm).

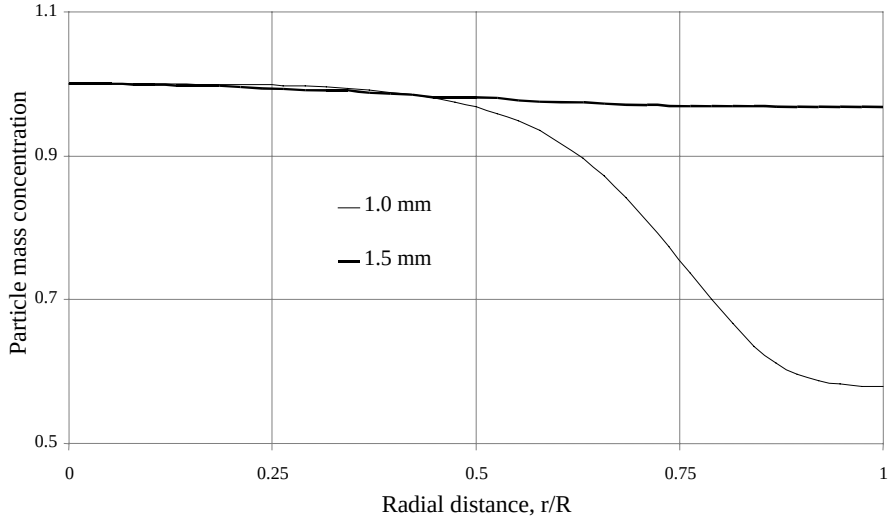

Fig. 8. Mass concentration distribution for different particle sizes (1.0 and 1.5 mm).

The distribution of mass concentration is shown in Fig. 8 for different particle sizes (1 and 1.5 mm). The mass concentration of the particles depends on their radial velocity shown in Fig. 6.

Comparison of the results

Comparing the results with our previous work "Numerical simulation of uprising gas-solid particle flow in circulating fluidized bed" [2], in which theoretical initial data was used, the following remarkable facts can be noticed:

- The 2D RANS approach gives a more comprehensive picture of description of phenomena in CFB than TBL (turbulent boundary layer approach) with respect to distribution of average velocity components of both phases, turbulent energy and particle mass concentration. The interparticle collision in the considered RANS method results in redistribution of velocities, turbulent energy and mass concentration not only in radial direction but in streamwise direction as well. The numerical results obtained for two cases with and w/o particle collision are qualitatively close but differ quantitatively underlining that in conditions of CFB operating with dense particle flow it is indispensable to take into account the effect of particles' collision.
- The particle mass concentration in our work is greater for the motion of coarse particles than for the small ones. It is caused by a big turbulence diffusion in the vicinity of the wall. Also, to make certain conclusions about particle mass concentration, the flow has to be fully developed, which is not the case here.

Conclusions

The numerical simulation of fluid dynamic processes under thermodynamic conditions was first performed by 2D RANS (Euler/Euler) approach which was applied for real-scale uprising CFB risers with solid ash particles of Estonian shale. The main contribution to the formation of the flow stemmed from the interparticle collisions and four-way coupling turbulence modulation due to the presence of solids. The other forces exerted on the motion of solids are gravitation, viscous drag and lift forces. On the basis of the performed calculations one can conclude that:

- rough particles generate a noticeable amount of turbulent energy producing much mixing processes in the flow domain;
- interparticle collisions along with the four-way coupling turbulence generate high level of turbulence considerably intensifying the process of particles' mixing and enhancing heat exchange between solid ash particles and gases.

Acknowledgement

The work was supported by a Grant No. ETF7620 of Estonian Science Foundation and by the target financing SF0140070s08.

Nomenclature

C – mass density of the dispersed phase (kg/m^3)
C_M – coefficient of Magnus force
C'_D – factor of drag coefficient
d – pipe diameter (m)
d_i – particle size of i-th fraction
f – friction
F_s – Saffman force (1/s)
g – gravitation acceleration (m/s^2)
k – turbulent energy (m^2/s^2)
k_n – coefficient of restitution
p – pressure (kg/m·s^2)
r – radial coordinate (m)
R – pipe radius (m)
T_* – characteristic time of hydrodynamic process (s)
u – axial velocity component (m/s)
$\overline{u}$ – gas velocity over cross-section (m/s)
v – radial velocity component (m/s)
v'_{si} – fluctuation radial velocity of dispersed phase
v''_{si} – normal particle's velocity after collision with the wall
x – axial coordinate (m)
Ω – angular velocity slip between gas- and dispersed phases (1/s)
α – particle mass concentration (kg/kg)
β – correcponding mass loading
δ – a particle diameter (μm)
ε – dissipation rate of turbulent energy (m^2/s^3)
λ – inter-particle spacing (m)
μ – dynamic viscosity (kg/m·s)
μ_d, μ_0 – dynamic and static friction coefficients of particle-wall collision
ν – kinematic viscosity (m^2/s)
ρ – density of gas (kg/m^3)
τ_c – inter-particle time of collision
τ_p – particle relaxation time
τ_i – response time for the "i" fraction of particles (s)
ω – angular velocity (1/s)
ω'_{si} – fluctuation angular velocity of dispersed phase

Σ – summation over all particle fractions
Δ – numerical step grid
E – numerical constant, E=8.41

Subscripts
c – collision
h – channel width
i – i-th particle fraction of dispersed phase
lag – average velocity slip
Mi – coefficient for Magnus lift force
p – particle
ri – slip velocity i-th velocity component
si – i-th fraction of dispersed phase
t – turbulent
w – wall
τ – particle's Stoksian response time
ω – rotation
ωi – angular velocity of i-th particle fraction
0 – parameters of single-phase flow & dynamic friction

Superscript
$'$ – fluctuation and post-collision

REFERENCES

1. *Ots, A.* Oil Shale Fuel Combustion. – Tallinn, 2006, 833 pages.
2. *Kartushinsky, A., Martins, A., Rudi, Ü., Shcheglov, I., Tisler, S., Krupenski, I., Siirde, A.* Numerical simulation of uprising gas-solid particle flow in circulating fluidized bed // Oil-Shale. 2009. Vol. 26, No. 2. P. 125–138.
3. *Hussainov, M., Kartushinsky, A., Mulgi, A., Rudi, Ü., Tisler, S.* Experimental and theoretical study of the distribution of mass concentration of solid particles in the two-phase laminar boundary layer on a flat plate // Int. J. Multiphas. Flow. 1995, Vol. 21, No. 6. P. 1141–1161.
4. *Hussainov, M., Kartushinsky, A., Mulgi, A., Rudi, Ü.* Gas-solid flow with the slip velocity of particles in a horizontal channel // J. Aerosol Sci. 1996. Vol. 27, No. 1. P. 41–59.
5. *Frishman, F., Hussainov, M., Kartushinsky, A., Rudi, Ü.* Distribution characteristics of the mass concentration of coarse solid particles in a two-phase turbulent jet // J. Aerosol Sci. 1999. Vol. 30, No. 1. P. 51–69.
6. *Kartushinsky, A., Michaelides, E. E.* An analytical approach for the closure equations of gas-solid flows with inter-particle collisions // Int. J. Multiphas. Flow. 2004. Vol. 30, No. 2. P. 159–180.
7. *Hussain, A., Ani, F. N., Darus, A. N., Mustafa, A., Salema, A. A.* Simulation studies of gas-solid in the riser of a circulating fluidized bed // Proceedings of

the 18th International Conference on Fluidized Bed Combustion, ASME Publication. 2005. P. 201–207.

8. Thermal Calculation of Power Generators (Standard Method). – Moskva: Energija, 1973. 295 pages [in Russian].
9. *Perič, M., Scheuerer, G*. CAST - A finite volume method for predicting two-dimensional flow and heat transfer phenomena. - GRS – Technische Notiz SRR. 1989, 89–01.
10. *Perič, M., Ferziger, J. H*. Computational Methods for Fluid Dynamics. – Berlin, Heidelberg: Springer-Verlag, 1996.
11. *Crowe, C. T., Stock, D. E., Sharma, M. P.* The particle-source-in cell (PSI-CELL) model for gas-droplet flows // J. Fluid. Eng-T. ASME. 1977. Vol. 99. P. 325–332.
12. *Helland, E., Occelli, R., Tadrist, L*. Numerical study of cluster formation in a gas-particle circulating fluidized bed // Powder Technol. 2000. Vol. 110, No. 3. P. 210–221.
13. *Sommerfeld, M*. Validation of a stochastic Lagrangian modelling approach for inter-particle collisions in homogeneous isotropic turbulence // Int. J. Multiphas. Flow. 2001, Vol. 27, No. 10. P. 1829–1858.
14. *Pfeffer, R., Rosetti, S., Lieblein, S.* Analysis and correlation of heat transfer coefficients and friction factor data for dilute gas–solid suspensions. – NASA Technical Note D-3603, 1966.
15. *Michaelides, E. E*. A model for the flow of solid particles in gases // Int. J. Multiphas. Flow. 1983, Vol. 10, No. 1. P. 61–77.
16. *Crowe, C. T., Gillandt, I.* Turbulence modulation of fluid-particle flows – a basic approach // Proc. 3rd Int. Conf. Multiphase Flows, Lyon, June 8–12, 1998. CD-ROM.
17. *Arro, H., Pihu, T., Prikk, A., Rootamm, R., Konist, A.* Comparison of ash from PF and CFB boilers and behavior of ash in ash fields // Proc. 20th Int. Conf. Fluidized Bed Combustion, China, May 18–21, 2009. P. 1054–1060.
18. *Ding, J., Lyczkowski, R. W., Sha, W. T., Altobelli, S. A., Fukushima, E*. Numerical analysis of liquid–solids suspension velocities and concentrations obtained by NMR imaging // Powder Technol. 1993. Vol. 77, No. 3. P. 301–312.
19. *Matsumoto, S., Saito, S. J*. Monte Carlo simulation of horizontal pneumatic conveying based on the rough wall model // J. Chem. Eng. Jpn. 1970. Vol. 3, No. 2. P. 223–230.
20. *Kartushinsky, A., Michaelides, E. E*. Gas-solid particle flow in horizontal channels: decomposition of the particle-phase flow and interparticle collision effects // J. Fluid. Eng-T. ASME. 2007, Vol. 129, No. 6, P. 702–712.

Received October 7, 2009